Flow visualization: state-of-the-art development of micro-particle image velocimetry

OPEN ACCESS
IOP Publishing
Measurement Science and Technology
Meas. Sci. Technol. **33** (2022) 092002 (17pp)
https://doi.org/10.1088/1361-6501/ac75b0

Topical Review

Flow visualization: state-of-the-art development of micro-particle image velocimetry

Amin Etminan*, Yuri S Muzychka, Kevin Pope and Baafour Nyantekyi-Kwakye

Department of Mechanical Engineering, Faculty of Engineering and Applied Science, Memorial University of Newfoundland (MUN), St. John's NL A1B 3X5, Canada

E-mail: aetminan@mun.ca

Received 30 December 2021, revised 24 May 2022
Accepted for publication 1 June 2022
Published 28 June 2022

Abstract

Experimental flow visualization is a valuable tool for analyzing microfluidics and nanofluidics in a wide variety of applications. Since the late 1990s, considerable advances in optical methods and image postprocessing techniques have improved direct optical measurements, resulting in an accurate qualitative and quantitative understanding of transport phenomena in lab-on-a-chip capillaries. In this study, a comparison of different optical measurement techniques is presented. The state-of-the-art development of particle image velocimetry (PIV) to date, particularly in microscale applications, is reviewed here in detail. This study reviews novel approaches for estimating velocity field measurements with high precision within interrogation windows. Different regularization terms are discussed to demonstrate their capability for particle displacement optimization. The discussion shows how single- and multi-camera optical techniques provide two-dimensional and three-component velocity fields. The performance of each method is compared by highlighting its advantages and limitations. Finally, the feasibility of micro resolution PIV in bioapplications is overviewed.

Keywords: flow visualization, experimental method, particle image velocimetry, transport phenomena, two-phase flow

(Some figures may appear in color only in the online journal)

1. Introduction

Fluid mechanics involves a wide range of scales governing the transport of momentum, heat, and mass. Therefore, a visual estimate of flow dynamics is an important tool to describe flow behavior qualitatively and quantitatively. Flow visualization provides significant and precise information about flow characteristics in space and time. It also provides investigators with data on the flow of interest to theorize and verify flow behavior. Several noninvasive flow visualization techniques have been developed in experimental fluid dynamics to provide data on fluid motions and their interactions with the surroundings. Flow visualization, in general, involves two categories: surface and off-the-surface methods. Each method has advantages and disadvantages.

* Author to whom any correspondence should be addressed.

Colored oils, nylon tufts, fluorescent dyes, and special clay mixtures, all placed within the medium of interest, respond to shear stress on the solid surface of an object, display flow patterns, and form streaklines around the object; this is called the surface flow visualization (SFV) technique. For example, fluorescent dyes or oil particles are illuminated when excited by ultraviolet light sources and maintain flow patterns on a wall (Barzegar Gerdroodbary 2020). This invasive technique provides an illustrative image of the flow around an object in laminar, turbulent, boundary layer transition, and flow separation by coating the outer surface of a model that is to be investigated with dyed oil or pressure-sensitive paint. SFV operates based on the principle that tracer particles faithfully follow the flow without any significant lag (Eck *et al* 2019). Owing to viscous effects, a fluid flow parallel to a surface causes a force along the surface, resulting in a wall or surface shear stress. The magnitude and direction of the fluctuating surface shear stress can be directly measured using a complementary surface method called surface or sublayer fence, first introduced by Patel (1965). The approach presented an improved high-precision curve calibration of the Preston tube with highly favorable and adverse pressure gradients. It also eliminated errors in earlier experiments, which were later adopted based on microelectromechanical systems (MEMS) by von Papen *et al* (2002) and Schober *et al* (2004). Hot-wire anemometry is a velocity measurement technique based on forced heat transfer from a heated wire which has also gained prominence in evaluating surface shear stress in both laminar and turbulent boundary layers (Ghouila-Houri *et al* 2017, 2019a, 2019b, 2021). Yang and Zhang (2021) summarized the state of the art in the flexibility of MEMS sensors that were no longer limited to mechanical rigidity by discussing 194 papers. This high-performance, bendable, and stretchable MEMS device can be used in a wide range of disciplines, such as mechanical engineering, electrical engineering, chemistry, and materials science.

As illustrated in figure 1, the oil/dye response technique offers a unique ability to capture flow streaklines around a model. The error depends on the choice of oil/dye employed and the extent to which the fence protrudes from the viscous sublayer adjacent to the model surface. Figure 1 shows time-history snapshots of the flow visualization and flow patterns over a triangular micro-ramp using a mixture of paraffin, fluorescent color powders, silicone oil, and oleic acid.

The optical flow visualization (OFV) method, an off-the-surface experimental flow technique, was designed based on the distribution of the light refraction index in a transparent fluid flow. Any changes in the intensity of the light beam passing through a fluid flow field would carry information to quantify the displacements or phase modulations. The optical refractive index is a function of the air density at each point, with the density as a function of velocity, pressure, and temperature (e.g. Ristić 2007, Smits and Lim 2012). This complex concentration of the optical refractive index is visualized by optical techniques, such as shadowgraphy, schlieren photography, and interferometry. Light attenuation or laser-induced fluorescence can be added to a fluid to create more visible flow

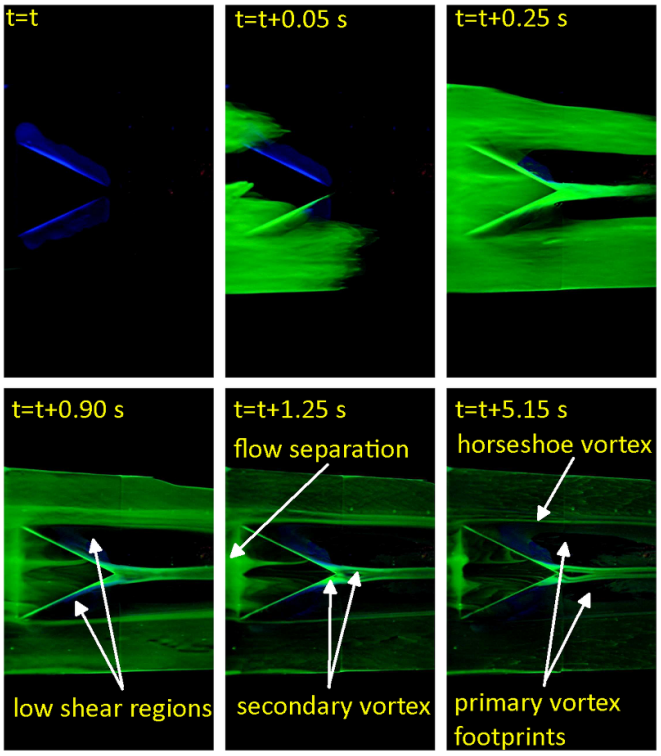

Figure 1. Chronological images of the SFV and flow patterns over a triangular micro-ramp with dimensions of width, cord, and height of 27.2, 33.4, and 4.64 mm, respectively, using a mixture of paraffin, fluorescent color powders, silicone oil, and oleic acid. The blue oil deposited around the ramp, as shown at the beginning, is just used for visibility. Then, the flow on the top surface of the micro-ramp moves towards the slant edges on both sides, which are caused by the high-pressure gradient created by the leading-edge shock wave (shown at $t + 0.05$ and $t + 0.25$ s). Therefore, as the flow rotationally moves down the slant edges, it casts large visible vortices on both sides. Downstream of the model, two wide areas are not covered with oil, and this is recognized to be the footprints of the primary vortices, shown at $t + 1.25$ and $t + 5.15$ s. Reproduced with permission from Saad (2013).

patterns (Settles 2001, Smits and Lim 2012). Table 1 presents a summary of three noninvasive OFV methods.

Particle tracking velocimetry (PTV), another off-the-surface experimental flow visualization method, can be used to measure the velocities and trajectories of moving particles added to the fluid flow. Typically, same-sized spherical tracer particles can be solid, liquid, and even gaseous and should be neutrally buoyant to follow the fluid motion and pathline with the lowest possible sedimentation and drag between the particles and bulk fluid, resulting in the most accurate visualization. Therefore, it is assumed that the velocities of the tracer particles and localized flow are the same, and the tracer particles' attributes are adjusted to the bulk fluid flow.

The PTV method can provide measurements in a two-dimensional (planar) slice of a fluid field illuminated by a thin laser sheet and a single camera or in a three-dimensional (volume) space of fluid flow based on volume illumination and a stereoscopic arrangement of multiple cameras (Merzkirch 1987, Schroeder and Willert 2008, Kreizer *et al* 2010). As

Table 1. Summary of three noninvasive OFV methods (Merzkirch 1987, Merzkirch and Ramesh 2000, Settles 2001, Ristić 2007).

Method	Refractive index	Optical equipment	Remarks
Shadowgraph	Density	• Light source • Recording plane	• Simplest method • Lowest optical sensitivity (mere shadows) • Suitable for transparent media • Suitable for qualitative description • Not suitable for quantitative measurements • Difference between localized brightening/darkening of light beams on the recording plane due to differences in density and temperature • Based on the light beam displacement • Sensitive to changes in the second spatial derivative of refractive index • Sensitive to the length of the light path • Complicated calculations due to a reduction in the dimension of the problem from 3D to 2D images of flow • Useful in the shock wave, aeronautical, aerospace, combustion, ballistic, explosion problems, and even in cough flow visualization
Schlieren	Density	• Light source • Recording plane • Concave mirrors • Knife-edge	• Suitable for transparent media • Suitable for qualitative description • Based on the light beam refraction angle • Sensitive to changes in the first spatial derivative of refractive index • Much higher resolution and sensitivity than shadowgraph (focused images) • Sensitive to cutoff (amount of light blocked by the knife edges) • The ability of color imaging utilizing color strip filters instead of knife-edge filters
Interferometry	Density	• Laser source • Achromatic lens • Mirrors • Reflection hologram • Spatial filter • Beam splitter cube	• Suitable for qualitative and quantitative descriptions • Sensitive to changes in absolute refractive index • Highest resolution and accuracy

the name implies, this technique tracks individual particles making it a Lagrangian approach, in contrast to particle image velocimetry (PIV) which uses the Eulerian approach (observing a point in space) to map the velocity field. A natural extension of the PIV technique from a two-dimensional to fully spatial measurements is defocusing digital PIV (DDPIV), which was first proposed by Willert and Gharib (1992), and its capability of measuring micro resolution velocity fields, called micro-DDPIV (μDDPIV), was developed by Yoon and Kim (2006) and Pereira *et al* (2007). A review study of μDDPIV furnished by a new regression-based multi-frame particle tracking algorithm was conducted by Kim (2012), where quantitative flow visualization of a complex velocity field in a chaotic mixer was presented as an example. Because the focus of this work is on micro-scale hydrodynamic measurements, the micro-PIV (μPIV) is described in the following sections, and the authors refer readers to prominent publications in the field for further comprehensive introduction of PTV and PIV (e.g. Schroeder and Willert 2008, Adrian and Westerweel 2011, Raffel *et al* 2018).

Since SFVs are limited by the presence of a solid surface, this study compares three OFV methods and then presents an in-depth review of the PIV diagnostic method by describing its recent development within different disciplines. State-of-the-art development of micron resolution PIV techniques has been studied in three categories: theoretical (method), technological, and applicability. The trends of current and probable future developments are discussed to outline the successful implementation of μPIVs in applications of interest.

2. Discussion on the recent developments of PIV

PIV is a well-developed and noninvasive optical measurement technique, particularly for multiphase flows, which has benefited from advances in computer-based control systems, high-precision timing, light sources (e.g. lasers, light-emitting diodes, and white light), and time-efficient image postprocessing software. A PIV system includes several essential components: seeding, illumination, recording, calibration, image evaluation and processing, and postprocessing.

The two main image-recording techniques are called single and multiple frames based on the quantity of images in the illuminated plane frame or the number of images for each illumination pulse (figure 2). As shown in figure 2, a single-frame/multi-exposure PIV recording technique superimposes several exposures at times t, t', and t'' to create a single image. Multiple-frame/single exposure recording techniques provide the temporal order of the particle images using high-speed

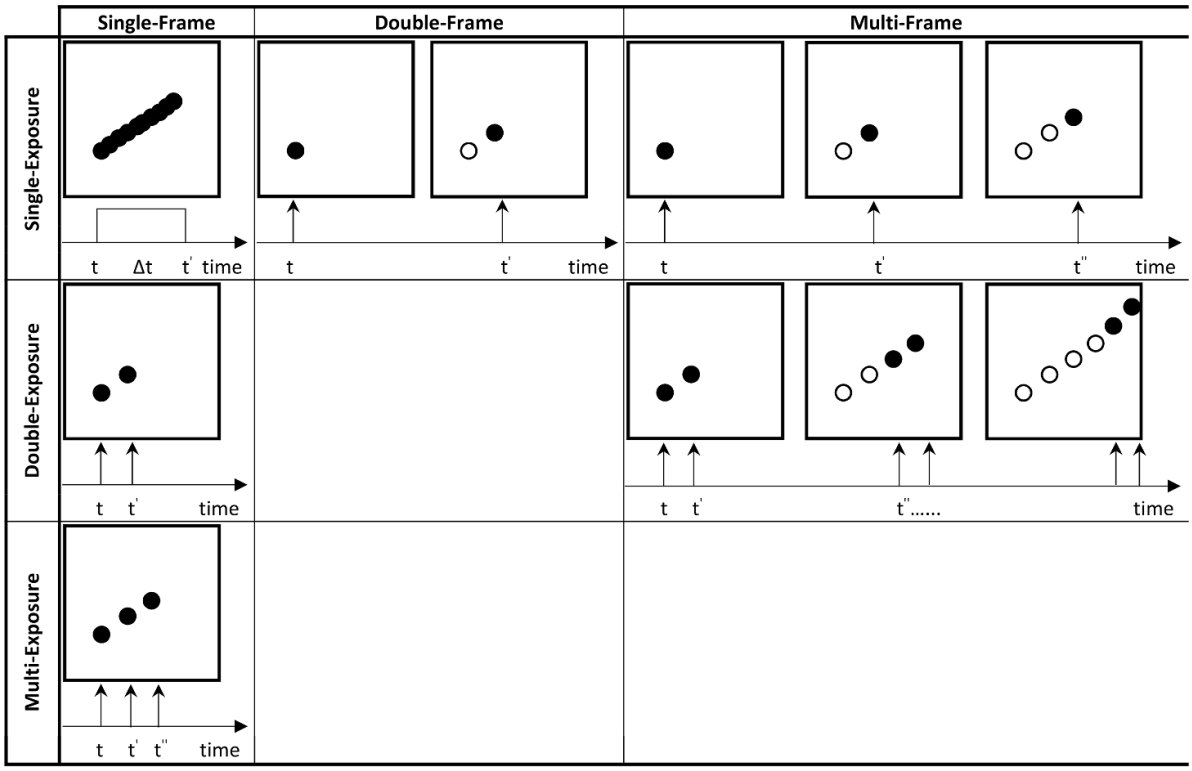

Figure 2. Single, double, and multiple-frame image-capturing techniques (open circle represents the position of the particle in the previous frame).

motion cameras. For instance, using a double-frame/single-exposure technique, as one of the most common photography techniques, seeding tracer particles are illuminated on a sheet of a double pulsed laser light twice over a very short and known time interval. The light scattered by the tracer particles creates two images (captured and recorded by a high-speed camera) from which particle displacements can be estimated in the flow. Technically, each frame can be split into a large number of areas of interest, called interrogation windows, where a displacement vector field can be calculated with the help of correlation techniques. The cross-correlation (CC) technique is more appropriate compared to the autocorrelation technique, for example, for calculating the instantaneous velocity at each point of interest when a double pulse laser light source is employed. Commonly, preprocessing techniques must be employed to minimize the influence of zero-displaced particle images created by the ratio of background noise to low-signal noise (Kirby 2010). Based on the depth of the flow field perpendicular to the viewing axis, PIVs can be classified into low- and high-density images, of which the latter lowers the out-of-focus images, increases the concentration of particles, and is much more compatible with low-depth flows, such as microchannels (Olsen and Adrian 2000, 2001). The displacement of particles between two subsequent images using the multiple-frame image-capturing technique can be reliably calculated by a sufficiently small time interval limited to 4–8 pixels (Raffel *et al* 2018). As a rule of thumb, the so-called one-quarter rule, the maximum displacement of a particle within an interrogation window should not be greater than 0.25 of the interrogation window extend in the direction of particle move; otherwise, uncertainty arises (Raffel *et al* 2018). Particle displacement is not dependent on the densities of the fluid and particle when the time interval is much longer than the particle inertial response time. Therefore, after evaluating the displacements of the particles within the two subsequent images and removing invalid measurements, the local instantaneous velocity vectors in the laser light sheet can be determined by dividing the estimated displacement by the calculated time between the image pairs.

The initial development of PIVs, especially after considerable advances in the method itself and equipment, and the high demands of implementation of PIV make it a systematic way to investigate transport phenomena over a broad dynamic range of systems that are not limited to fluid mechanics and aerodynamics applications. Before reviewing μPIV in capillaries, it will be relevant to highlight the relevance of using the PIV system to conduct both fundamental and practical measurements over a wide range of topics. Some of these relevant studies have been published in highly rated journals. Two journals, called *Experiments in Fluids* (https://springer.com/journal/348), and *Measurement Science and Technology* (https://iopscience.iop.org/journal/0957-0233), are selected based on two basic principles: new developments of the PIV and innovative applications. The dissemination of papers dealing with the PIV systems in the previously mentioned peer-reviewed journals over the past two decades is addressed in the following. These journals showed significant dedication to PIVs, resulting in 92 and 21 articles, respectively. Despite the ongoing COVID-19 pandemic, declared by the

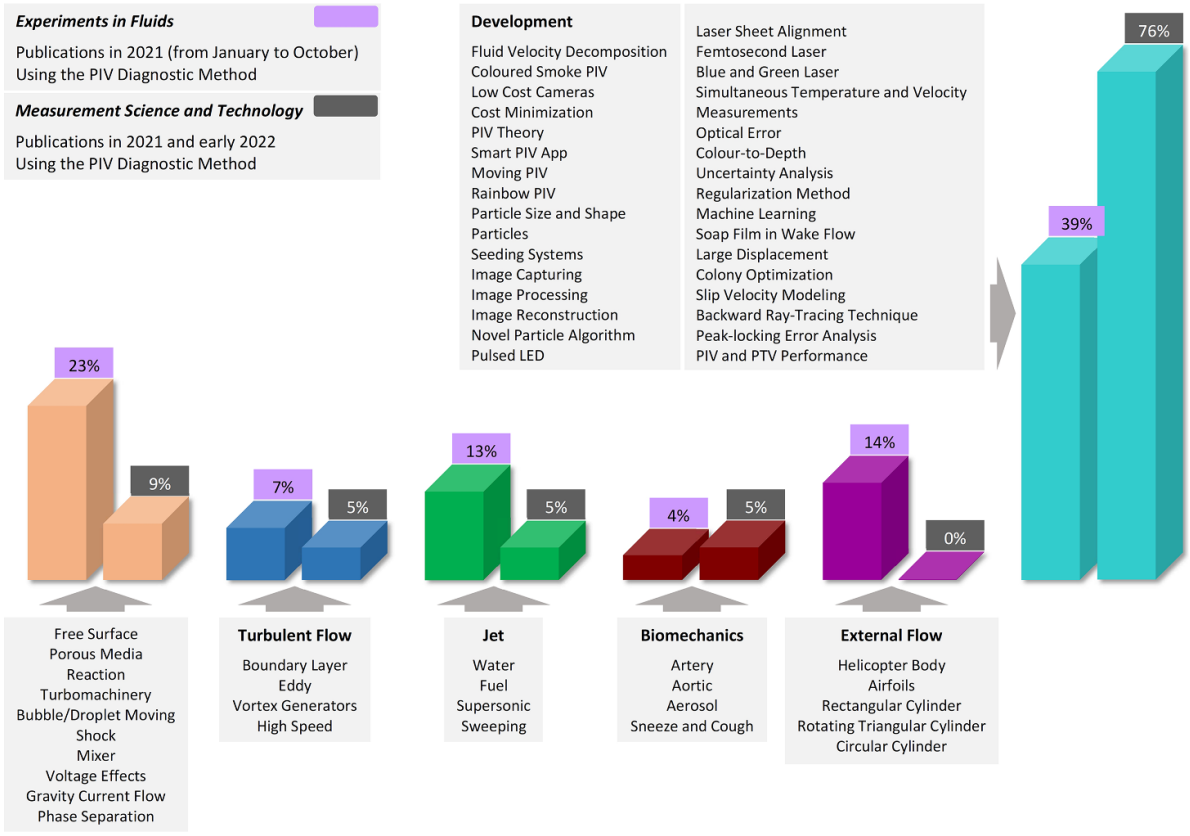

Figure 3. Statistical analysis of the number of papers published by *Experiments in Fluids* and *Measurement Science and Technology* that deal with the PIV diagnosis method.

World Health Organization, due to the novel coronavirus SARS-CoV-2 on 11 March 2020, the number of publications in these journals has increased and also effectively expanded into microscopic and macroscopic biomedical applications because of its ability to answer various research questions (e.g. Bahl *et al* 2020, de Silva *et al* 2021, Haffner *et al* 2021, Tan *et al* 2021). The state of recent developments in the PIV diagnostic technique by a statistical analysis of 92 and 21 papers published by *Experiments in Fluids* and *Measurement Science and Technology*, respectively, in 2021 (and early 2022 for the last journal) is carried out by showing the contribution percentage of six categories employing the PIV systems to provide deep insights into transport phenomena (figure 3). As shown in figure 3, the majority of studies are focused on the development of PIVs within a broad classification, which can be divided into three groups, namely theoretical aspects (e.g. PIV theory, method, image processing, and uncertainty analysis), technological aspects (e.g. laser light, particles, and seeding system), and applicability (e.g. biomechanics, jet, and phase separation). There are, however, other types of developments beyond imagination, such as the growth of PIVs. For instance, Cierpka *et al* (2021) introduced an app compatible with smartphones to capture and record velocity fields with lower complexity and cost than conventional PIV systems, which can be used for educational purposes. Consequently, theoretical and technological developments in PIVs have drawn much more attention from researchers than their development in complex-flow applications. In addition to the aforementioned journals, several international symposia have showcased significant attempts in the development of PIV systems in various research areas that are being continuously expanded. Some of the highly anticipated international conferences identified are the 14th *International Symposium on Particle Image Velocimetry* (www.iit.edu/ispiv2021), the 19th *International Symposium on Flow Visualization* (https://isfv2020.sjtu.edu.cn/index), and the *2021 Micro Flow and Interfacial Phenomena (μFIP) Conference* (https://microfip2021.wustl.edu/), that were all held virtually due to the COVID-19 global pandemic.

Figure 4 presents three subjective breakthroughs: theoretical, technological, and applicability that happened to the PIV developments resulting in significant progress over the past two decades. Advances in PIV systems are interdependent with considerable progress under each breakthrough, which are carefully reviewed under the development of micro-resolution PIV section in this article.

3. Micro PIV (μPIV)

Micron-resolution PIV is an efficient technique for visualizing an in-depth description of microfluidic applications using fluorescent particles as small as several hundred nanometers. The tremendously small size of the particles predisposes the

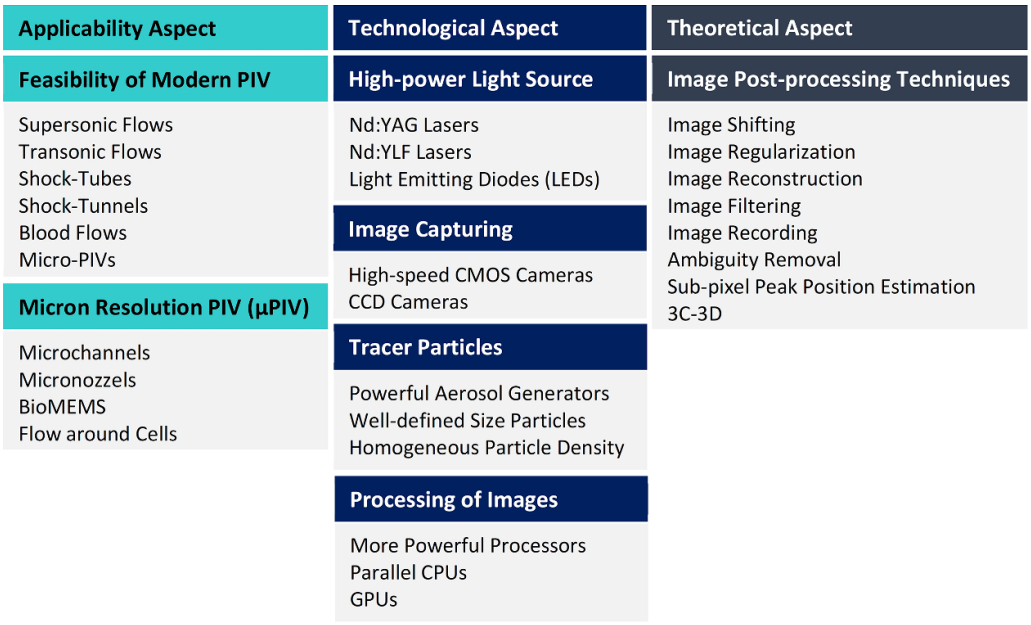

Figure 4. Three major milestones: applicability, technological, and theoretical aspects of the PIV systems summarized in seven subcategories over the past two decades.

Brownian motion of particles to be in line with the bulk fluid motion. This gives rise to a one-micron resolution for microscopic image capturing (Santiago *et al* 1998, Meinhart *et al* 1999, Kirby 2010). In μPIVs, a lower particle density and illuminated volume instead of an exact two-dimensional light sheet make it more challenging to use compared to conventional PIVs. An illustrative experimental setup of CC μPIV in a typical microfluidic laboratory (figure 5) includes a fluid supply unit, microfluidic device, microscopic unit, laser light source, synchronous controller, and μPIV data processor. The principle of operation is similar to that of conventional PIV, in that neodymium-doped yttrium aluminum garnet laser light is reflected through a dichroic mirror and travels through an objective lens focused on the focal panel of interest in a flow model to illuminate a specific flow volume. The reflected laser beams and emissions from the particles travel back through the lens, dichroic mirror, and an emission filter called a barrier filter, which prevents the laser beams from passing. Fluorescent nanoparticles reflect laser beams at a longer wavelength than the absorbed light. A high-speed charge-coupled device camera captures and sends numerous images for processing (Kirby 2010). An adequate depth of flow field of the camera maximizes the in-focus particle images and minimizes the scattered light of out-of-focus illuminated particles.

Image resolution is key to the quality of the data obtained from any μPIV setup; hence, effective measures are required to ensure the capture of highly resolved images. To date, the two main factors identified to adversely affect image resolution and reliability are wall overshadowing and hydrodynamic interactions between the wall and seeding particles (Meinhart *et al* 1999). The former factor results in background reflection, which induces significant uncertainty in the determination of the exact position of the wall. The latter factor pushes particles away from the boundary layer and causes a lack of velocity-field measurements over the near-wall region. The dominance of any of these factors will result in measurement errors, which will propagate throughout the experiment and adversely affect the higher-order moments desired to completely elucidate the flow physics. Therefore, mitigating these occurrences is critical. The epifluorescence method and flow-tracing particles with diameters of 200 nm can resolve the effects of these two destructive factors (Meinhart *et al* 1999).

Polydimethylsiloxane (PDMS) is the most common material for constructing microchannels or lab-on-a-chips with several specific properties, such as easy-to-fabrication, mechanical flexibility, transparency, adaptability to a wide range of chemical applications, and chemical inertness. Photolithography is a common method for fabricating a prototype microchannel using PDMS (Duffy *et al* 1999, Beebe *et al* 2001, Whitesides *et al* 2001). The μPIV method is utilized for numerous applications, such as lab-on-a-chip, pharmacological, bioMEMS, biomedical, microreactor, microchemical, and analytical chemistry.

3.1. Theoretical (method) development

Flow visualization techniques have been efficiently expanded to a broad range of topics in fluid mechanics, owing to significant technological advancements. This section of the current review deals with the theoretical development and mathematical interpretation of image processing using μPIV systems.

Particle displacement estimation results in a velocity vector field, providing researchers with precise two-dimensional and three-dimensional flow structures. Double-frame/single-exposure images must be processed to determine the exact displacement of each particle within a specified time interval. Therefore, a CC function $R(\mathbf{s})$, an efficient measuring

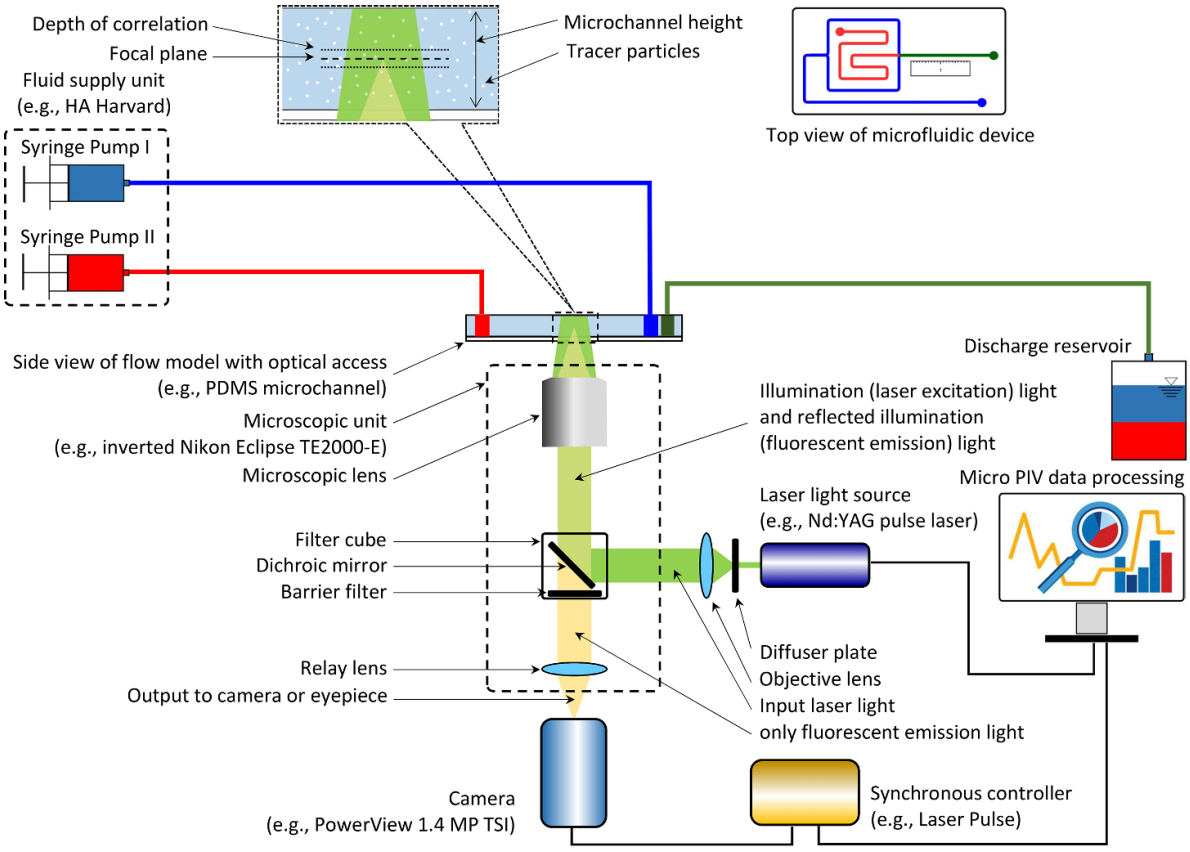

Figure 5. Schematic illustration of the μPIV system in the *Microfluidic Laboratory* at the *Memorial University of Newfoundland*. A pair of high-precision syringe pumps establish a continuous, steady, and pulsation-free two-phase Taylor flow in a microfluidic device with a cross-junction (the top view of the flow model is shown at the top right). The microscopic lens focuses the laser excitation light on a two-dimensional plane with a thickness known as the depth of correlation (shown at the top left). The accuracy of the correlation is significantly attributed to the reflection of the tracer particles.

tool, was introduced to find the similarities between two consecutive images and show the displacement ($\mathbf{s}$) of the particles in one image relative to the other (Adrian 1988, Willert and Gharib 1991, Keane and Adrian 1992, Westerweel 1997),

$$R(\mathbf{s}) = R_{\mathrm{C}}(\mathbf{s}) + R_{\mathrm{F}}(\mathbf{s}) + R_{\mathrm{D}}(\mathbf{s}) \tag{1}$$

where $R_{\mathrm{C}}(\mathbf{s})$, $R_{\mathrm{F}}(\mathbf{s})$, and $R_{\mathrm{D}}(\mathbf{s})$ are the convolution of the mean image intensity, fluctuating noise arising from the difference between the mean and fluctuating image intensities, and Gaussian intensity distribution function for showing the Gaussian peak shape of the velocity in the images, respectively (Adrian 1988, Keane and Adrian 1992). The primary measurement errors are attributed to the diameter, intensity, and contrast of the particles, out-of-plane, and even in-plane displacements within the interrogated velocity field windows. The three-point Gaussian intensity distribution over interrogation windows was first introduced by Willert and Gharib (1991) for the peak interpolation and is still efficient practical.

A significant breakthrough in CC has occurred since the 2000s through new mathematical concepts to increase the image acquisition quality conducted with PIV systems (Meinhart *et al* 2000). Meinhart *et al* (2000) demonstrated that the contributions of other displacement components might affect measurements and cause an erroneous estimation of the average velocity field. Thus, it is necessary to apply averaging methods to the data to estimate the averaged velocity vector fields, which are presented in figure 6 for an image sequence of N single-frame/double-exposure particle images (i.e. images A and B) within a known time interval Δt. These averaging methods calculate more accurate velocity fields with lower erroneous measurements than a standard CC, which creates an instantaneous velocity field with noisy and unreliable measurements in low-density particle images and near-wall regions (Meinhart *et al* 2000). The lack of low-density particle images can be compensated for in conventional μPIV measurements by performing these averaging methods.

An alternative to CC is the OFV technique, which computes velocity fields with high accuracy and spatial resolution due to remarkable advances compared to the development of CC-based PIVs. Moreover, a major source of estimation errors in CC-based approaches has been attributed to the smoothing effects of the interrogation window, which can be improved by applying a regularization term in optical flow calculations (Seong *et al* 2019, Simonini *et al* 2019). The regularization process has been well established in imaging-based velocity field measurements by adding a data term (J_{D}) and regularization term (J_{R}) within the particle displacement equation to obtain an optimized and accurate solution. The mismatch between a pair of images can be penalized by J_{D}

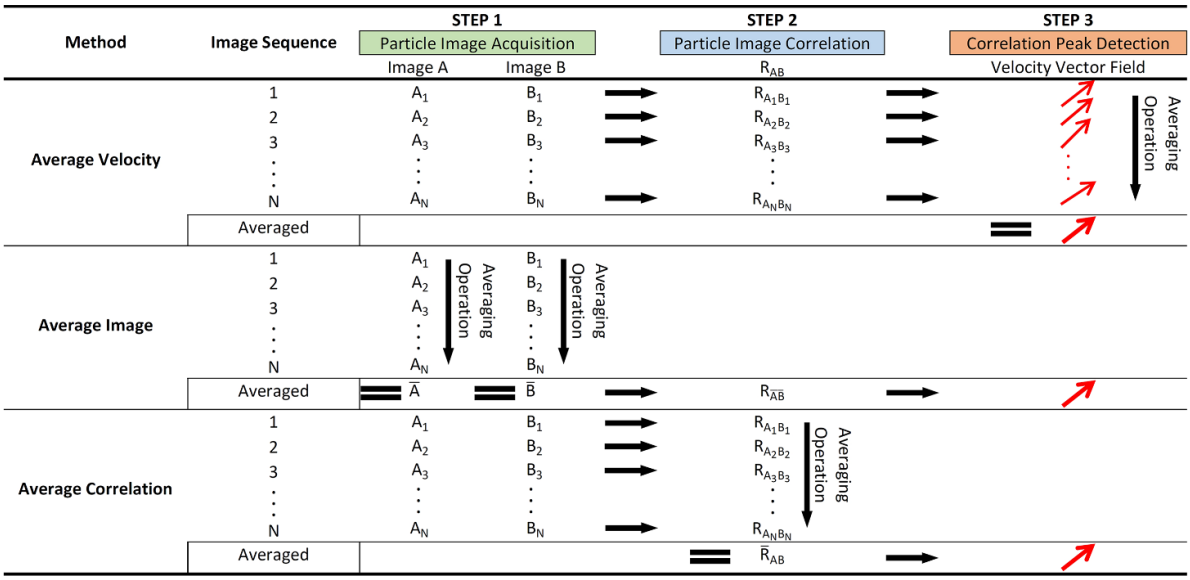

Figure 6. An illustrative schematic of three methods of predicting average velocity vector fields using a linear averaging operator after correlation peak detection in the average velocity method, after particle image acquisition in the average image method, and after particle image correlation in the average correlation method. Reproduced with permission from Meinhart *et al* (2000). © 2000 The American Society of Mechanical Engineers.

and the predicted velocity vector field ($\underline{v}$) can be smoothed/constrained by J_R (Schmidt and Sutton 2021). Table 2 lists the different regularization terms used in the literature. The importance of the regularization term is highlighted in regions of the interrogation window with a significant velocity gradient, such as vortices, shock waves, recirculation flows, and boundary-layer flows (Seong *et al* 2019). It is noticed that the use of regularization in image processing reduces the complexity of computations compared to statistical OFV methods.

Traditional PIVs often employ CCs to calculate the displacement field of two consecutive interrogated images called initial and moved projections on a two-dimensional plane. Table 3 presents a summary of two displacement measurement approaches by noting the advantages and disadvantages of each method.

To obtain a reliable flow dataset and velocity field, OFV methods require precise image processing to be conducted. An essential part of each OFV is to show the flow patterns using streamlines and stream surfaces. To address this need, convolutional neural networks (CNNs) and deep machine learning (ML) techniques have been effectively developed, which explicitly normalize a flow field, in particular, flow-based generative model, and leverage OFVs used in PIVs (Rezende and Mohamed 2015, Baker and Einav 2021, Chun-Yu *et al* 2021, Lagemann *et al* 2021, Yu *et al* 2021). Missing data recovery is crucial in image processing and typically occurs because of shadow and out-of-focus particle emissions within interrogated windows. Akbari and Montazerin (2022) employed ML to reconstruct the velocity field of turbomachinery PIV measurements with 25% clustered missing data. Multi-layer perceptron (MLP) and support vector regression (SVR) algorithms handle the nonlinear modeling of transport phenomena attributed to such turbomachinery flow fields, resulting in higher reconstruction accuracy of SVR compared to MLP due to its robustness and superior flexibility in ML (see also Higham *et al* 2016, Saini *et al* 2016, Wen *et al* 2019).

Flow instability caused by shear flow is dominantly responsible for the macroscale vortex structures that govern the linear and nonlinear behaviors and interactions of such coherent vortex structures (Lumley 1981). Tracking and characterizing macroscale coherent structures are still challenging parts of flow visualization involving vortices. Stevens and Sciacchitano (2021) introduced a novel ML method that combined clustering (i.e. an unsupervised technique to find clusters with similar properties) and the Hungarian algorithm and was independent of scale and could be used over different length scales. This method was designed to accurately estimate the temporal and spatial resolutions using consistent vortex labeling and tracking. A comprehensive review of ML for fluid mechanics problems was conducted by Brunton *et al* (2020). They distinctly addressed the success of ML in modeling, data-driven optimization, and multiscale flow visualization. Table 4 presents several deep ML and neural network techniques that are used to reconstruct the flow field.

Although the use of averaged correlations provides the mean particle displacement, i.e. the velocity vector field, within an interrogation window of a pair of two consecutive images, it is responsible for the lack of information on flow structures smaller than the interrogation window and high velocity-gradient regions. To overcome this weakness, single-pixel ensemble PIV (SPE-PIV) has been developed to measure pixel-wise CC from sequential images in contrast to a sequential pair of images obtained using conventional μPIVs (Westerweel and Scarano 2005). This technique of SPE-PIV (to measure the in-plane velocity field) and dual-plane illumination (to measure the out-of-plane velocity field) is able to determine two-dimensional three-component (2D3C) velocity field measurements (e.g. Noto

Table 2. Forms of regularization terms in the literature.

Name	Regularization term[a]	Remarks	References
Horn and Schunck (HS)	$J_{\mathrm{R}}^{\mathrm{HS}} = \int_{\Omega} \| \underline{\nabla} v_1 \|^2 + \| \underline{\nabla} v_2 \|^2 \mathrm{d}\underline{x}$	• The most common regularization term • Equivalent to first-order Tikhonov regularization • Penalizing the curl of velocity (i.e. vorticity) • Inappropriate for turbulent flows	Horn and Schunck (1981), Corpetti *et al* (2006)
Corpetti (d–c)	$J_{\mathrm{R}}^{\mathrm{d-c}} = \int_{\Omega} \| \underline{\nabla}(\underline{\nabla} \cdot \underline{v}) \|^2 + \| \underline{\nabla}(\underline{\nabla} \times \underline{v}) \|^2 \mathrm{d}\underline{x}$	• Equivalent to second-order div-curl regularization • Considering divergence and vorticity to be cohered • Without any firm basis considering a real fluid motion • Minimizes the gradients of the divergence and vorticity	Corpetti *et al* (2002), Yuan *et al* (2007) Schmidt and Sutton (2020)
Viscous fluids (μ)[b]	$J_{\mathrm{R}}^{\mu} = \int_{\Omega} \| \underline{\nabla}^2 \underline{v} + \frac{1}{3} \underline{\nabla}(\underline{\nabla} \cdot \underline{v}) \|^2 \mathrm{d}\underline{x}$	• Obtained directly from Navier–Stokes equation • Penalizing the derivatives in the same way of viscosity imposed	Schmidt and Sutton (2021)
Laplacian (Lap)	$J_{\mathrm{R}}^{\mathrm{Lap}} = \int_{\Omega} \| \underline{\nabla}^2 \underline{v} \|^2 \mathrm{d}\underline{x}$	• For divergence-free conditions • Commonly used in image filtering and smoothing • Not common in the OFV	Paris *et al* (2011), Kadri-Harouna *et al* (2013)
Helmholtz decomposition (Helm)	$J_{\mathrm{R}}^{\mathrm{Helm}} = \int_{\Omega} \| \underline{\nabla}^2 \underline{v} \|^2 + \| \underline{\nabla}^2 \underline{\chi} \|^2 + \| \underline{\nabla}^2 \underline{\boldsymbol{\theta}} \|^2 + \| \underline{\nabla}^2 \underline{\boldsymbol{\xi}} \|^2 \mathrm{d}\underline{x}$	• Considering four motion components: translation, linear distortion, shear distortion, and rotation • Considering physical properties of flow • Considering an increase in regularization parameters within regions with uniform change in intensity and a decrease in the image edges	Lu *et al* (2021)

[a] Where ∇, Ω, υ, $\boldsymbol{\chi}$, $\boldsymbol{\xi}$, and $\boldsymbol{\theta}$ are the gradient operator, two-dimensional image domain, velocity vector, linear distortion rate tensor, rotation tensor, and shear distortion rate tensor, respectively.
[b] This name has been selected by the authors of this study and obtained from the process of derivation of the regularization term conducted by Schmidt and Sutton (2021).

Table 3. Summary of displacement measurement approaches to extract velocity field through PIV.

Approach	Remarks	References
CC	**Advantages:** • Most frequently used traditional algorithm • Most commonly used benchmarking algorithm • Maximum spatial correlation used between two consecutive particle images • Adaptable to fast Fourier transform to lower computation expenses • Adaptable to an iterative algorithm called window deformation iterative multi-grid to improve robustness and accuracy **Disadvantages:** • Sparse velocity field • Postprocessing methods to reduce error vectors	Westerweel (1997), Scarano (2002), Westerweel and Scarano (2005), Raffel *et al* (2018)
OFV	**Advantages:** • Adaptable to anisotropic smoothness constraints to enhance accuracy • Adaptable to the dynamic programming to improve accuracy and spatial resolution by including order and continuity constraints • Adjustable to the brightness constraint equation • Flexible to physical knowledge and the geometry of problems **Disadvantages:** • Huge computational expenses and time-consuming • Dissatisfying understanding between the optical flow field and actual fluid velocity field	Nagel and Enkelmann (1986), Quénot *et al* (1998), Ruhnau *et al* (2005), Liu *et al* (2015)

and Tasaka 2021). Figure 7 illustrates the concept behind dual-plane SPE-PIV measurements. This method used two blue and red laser sheets with an offset depth of Δz and performed the capability of three-component velocity-field measurements at two in-plane and out-of-plane pixel by pixel. To summarize volumetric flow visualization, table 5 presents the advantages and disadvantages (limitations) of 2D3C PIV methods.

Table 4. Summary of different deep machine learning techniques used in flow field reconstruction.

Technique	Main remark	References
Convolutional neural network (CNN)	Low error rate for classifying images by a factor of two	Zitová and Flusser (2003), Krizhevsky *et al* (2012),
Deep CNN	Measurement of original displacement by a four-level regression	Lee *et al* (2017), Rabault *et al* (2017),
Fully-connected NN	Prediction network by six layers	Rabault *et al* (2017),
Artificial neural network	Accurate velocity field from a simple subwindow by the training data	Gu *et al* (2021)
Vector field reconstruction for unsteady flow data	Refined and denoise vector field by recurrent residual blocks	

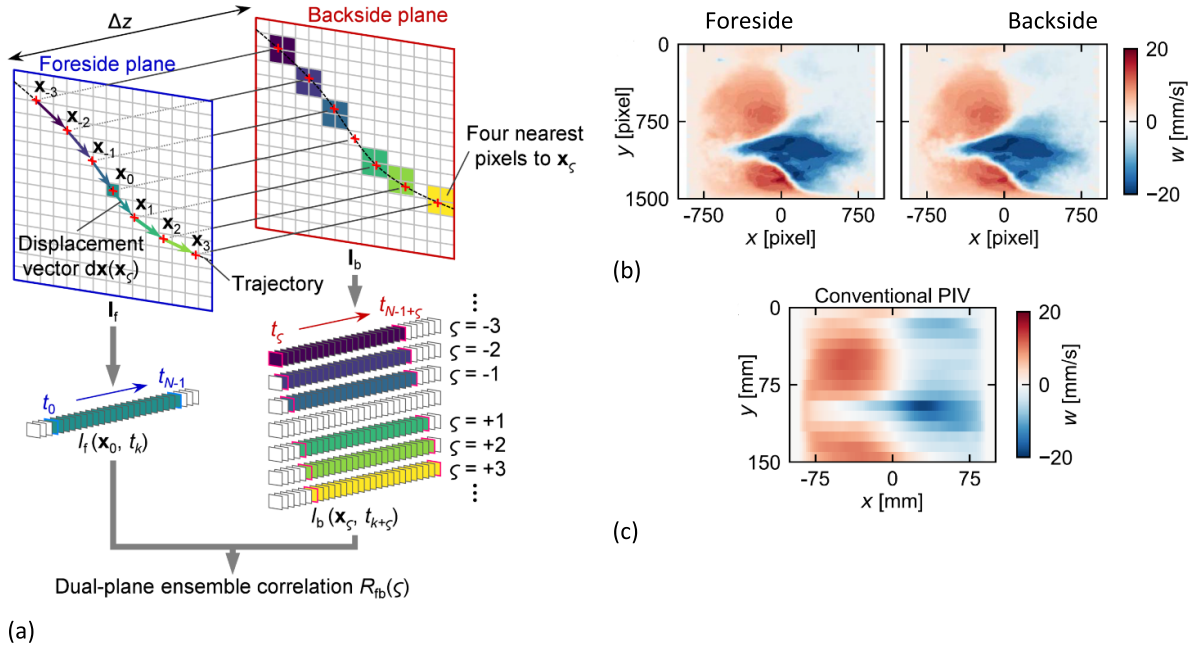

Figure 7. (a) An illustrative schematic of dual-plane correlation in SPE-PIV measurements. Two adjoining two-dimensional planes, i.e. the foreside and backside planes, were situated at a depth offset of Δz. An arbitrary particle with no negligible out-of-plane velocity component (w) passes position $\boldsymbol{x}_0 = (x_0,\ y_0)$ in the foreside plane at time frame $t = t_0$ and then through position $\boldsymbol{x}_\varsigma$ in the backside plane at the time frame $t_0 + \varsigma\Delta t$. (b) Out-of-plane velocity component field in two offset planes with a depth of 1 mm in the foreside (left) and backside (right) planes, (c) velocity field obtained by conventional PIV. Reproduced from Noto and Tasaka (2021), with permission from Springer Nature.

The flow regime in microfluidic applications is often laminar, enabling PIVs to obtain highly resolved images; however, this is limited to steady flow. To overcome this limitation, Kislaya *et al* (2020) introduced a novel method called Ψ-PIV, which requires a lower number of images (i.e. by eight times for steady and by 30 times for unsteady flow), particle density, and signal-to-noise ratio compared to traditional μPIV. Figure 8 shows the main differences between μPIV and Ψ-PIV. μPIV typically uses a large number of frames (i.e. 100–1000 frames) to be correlated and then averaged to predict the velocity field. Conversely, Ψ-PIV required significantly fewer frames (approximately ten frames) to obtain the local flow direction (Θ). Therefore, stream functions were obtained by following virtual particle paths along with the measured directions and then interpolating neighboring pathlines. Eventually, the velocity field is assigned by space differentiation of the stream function in terms of the distance between two consecutive interrogation windows. There are three main sources of noise that arise from velocity time-dependency, quantization (pixelization), and non-uniform velocity distribution within the interrogation window to perform measurements in turbulent flows. As mentioned earlier, the flow regime in microdevices remains laminar, for which a key noise analysis was conducted by George and Stanislas (2021).

3.2. *Technological development*

Due to technological limitations in the optical visualization of non-transparent flows, such as blood and slurry, the difference between the optimal and suspension particle image sizes is significant and must be improved. Refractive index-matching techniques, for example, self- or commercially-labeled particles, create a florescent rim- and plateau-shaped,

Table 5. Literature on single- and multi-camera 2D3C PIV.

Method	Remarks	References
Monography-PIV (single camera)	**Advantages:** • Simplified laboratory apparatus setup and calibration • Encoding particle depth on the camera side or illumination side • Reconstructing 3D particle paths in terms of position and length of captured images **Disadvantages:** • Low-resolution reconstruction due to angular information in image capturing • Low-frame rates in image capturing • Not-suitable for non-stationary fluid flow measurements • Highly sensitive to light scattering, random noise, and optical misalignment • Low depth-to-width ratio	Willert and Gharib (1992), Pereira and Gharib (2002), Yoon and Kim (2006), Fahringer *et al* (2015), Shi *et al* (2016)
Tomography-PIV (multi-camera)	**Advantages:** • The ability to deal with high-density tracer particles • The ability to provide high-resolution reconstruction images • Applicability over a wide range of flow phenomena • Adaptable to smartphones to reduce setup expenses • High axial resolution **Disadvantages:** • The complexity of a multi-camera system (i.e. 4–6 cameras) • Precise calibration to keep the high-quality reconstruction • High-power light source to illuminate a large depth-of-field	Elsinga *et al* (2006), Scarano (2012), Rice *et al* (2018), Shi *et al* (2018)
Rainbow-PIV (single camera)	**Advantages:** • Utilizing an illumination module to create a rainbow light pattern. • The ability to provide all-in-focus images of color-coded tracer particles. • The ability to reconstruct particle distributions and velocity fields. • Extendable depth-to-width ratio by changing rainbow thickness and adjusting optics. • The capability of velocity field reconstruction in low/non-uniform particle densities compared to tomography-PIV. **Disadvantages:** • Lower depth resolution in higher depth-to-width ratios • Limited axial resolution	Xiong *et al* (2017), Xiong *et al* (2021)

respectively. Using the fit functions of experimental data (e.g. smoothing spline), other distribution functions can be obtained, such as ring- and plateau-shaped distribution functions (Blahout *et al* 2021). Figure 9 shows the images of a particle utilizing three distribution functions.

Fragile equipment, laboratory-based, and pollutive tracer particles are the three main concerns of using μPIV and PTV techniques in the actual field, particularly in harsh environments. Recent field study developments, such as a compact open-source remotely-operated vehicle (ROV) and rising air bubbles as tracer particles for image capturing, make these methods efficient for portable technology and environmentally friendly velocity-component measurements (Løken *et al* 2021). A novel approach for measuring a reliable high-resolution velocity field under extreme Arctic conditions was recently introduced by Løken *et al* (2021). They employed PTV and PIV to track the motion of rising bubbles individually in the laboratory and the field, respectively, so they called the method remotely-operated vehicle particle velocimetry (ROV-PV). As pointed out by Løken *et al* (2021), a two-dimensional plane of rising bubbles enables ROV-PV to work without a light sheet but challenges the method with the strong buoyancy motion of the bubbles. Due to the non-uniform distribution of bubbles in terms of size and inertia, their method showed a relative error of 10% in the measurement of the horizontal velocity component.

3.3. Applicability development

The ability to visualize blood flow with the micron spatial resolution is of significant interest. Blood travel starts from the heart and then through the arteries, capillaries, and veins, i.e. from a high-pressure region to a low-pressure region. Capillaries are a complex network of microchannels between

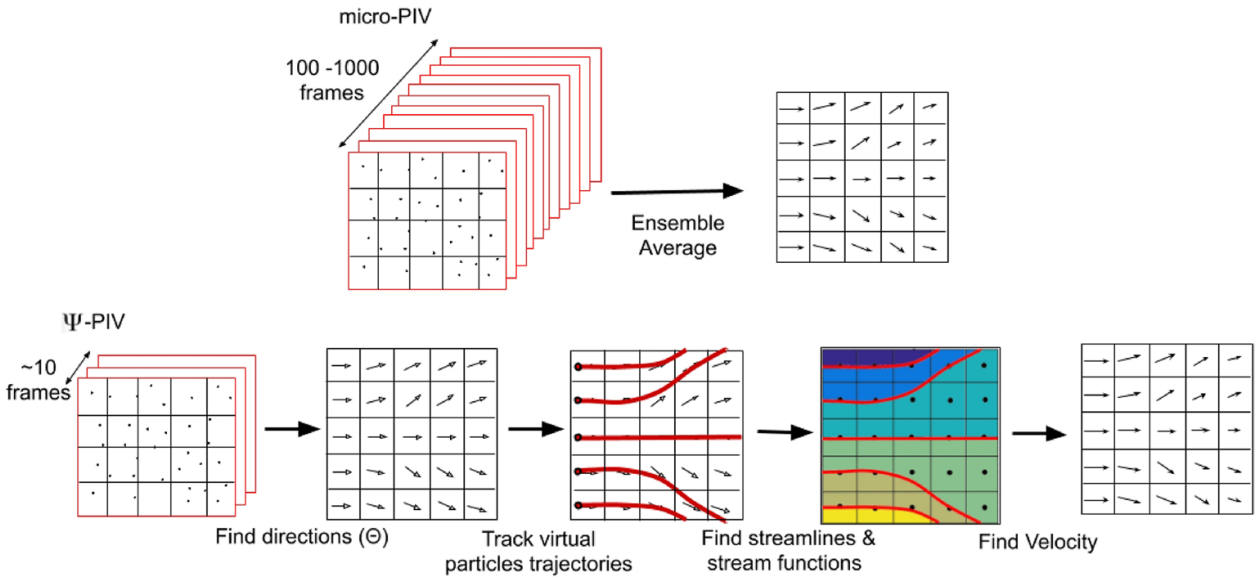

Figure 8. A schematic diagram showing the main difference between μPIV and Ψ-PIV. Reproduced from Kislaya *et al* (2020), with permission from Springer Nature.

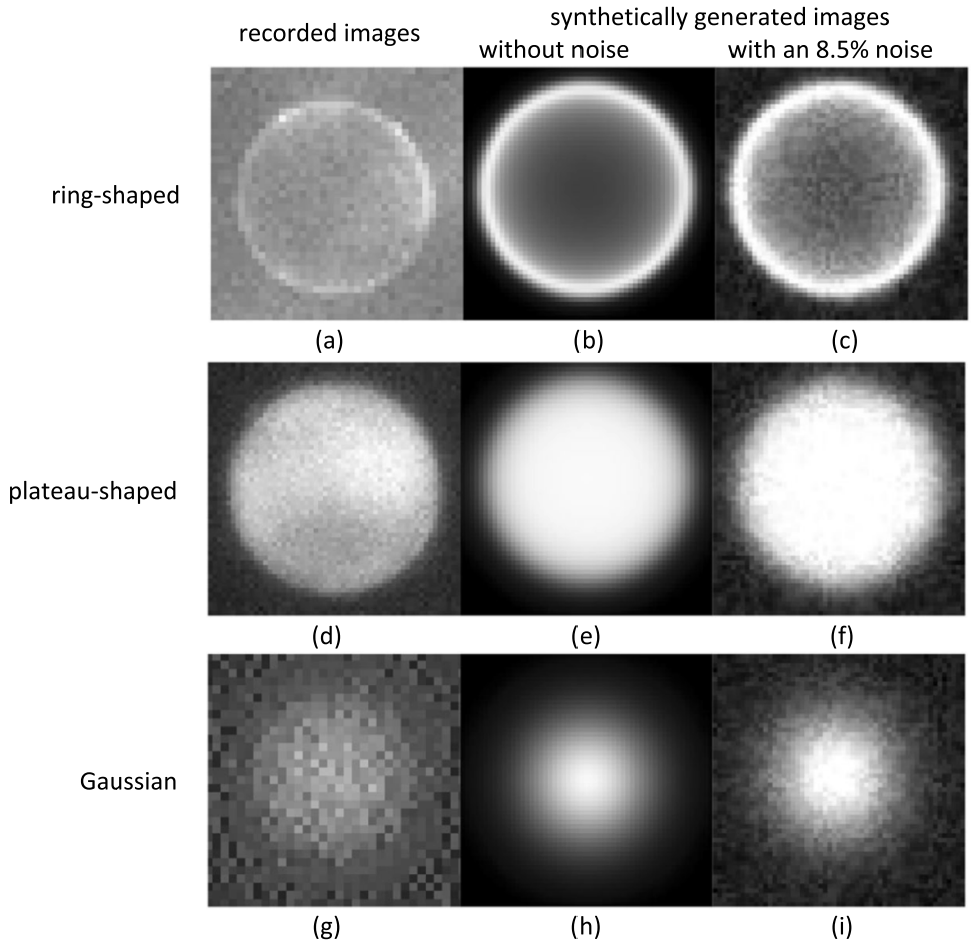

Figure 9. Effects of three CC distribution functions for predicting particle shapes. Synthetic particle shapes were generated by employing the smoothing spline fit function of the recorded image data, whereas the Gaussian fit followed an analytical intensity function. An 8.5% noise level was applied intentionally to consider the actual noise in the experimental image data. For synthetically generated images, self-labeled and commercially-labeled polymethylmethacrylate particles with a diameter of 60 μm are used, which perform ring- and plateau-shaped images of the particles. Reproduced from Blahout *et al* (2021), with permission from Springer Nature.

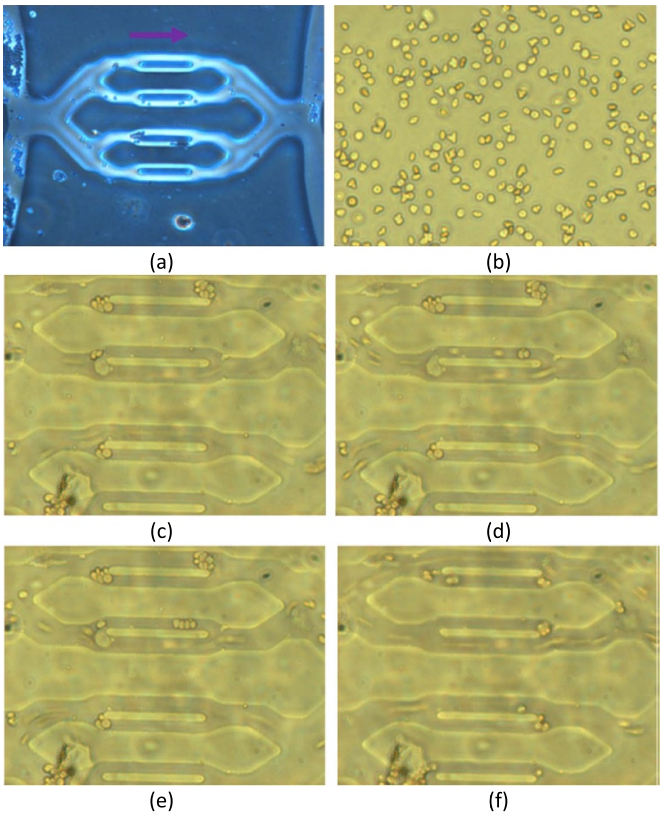

Figure 10. Optical microscopic images of (a) a complex capillary network carrying RBC solution, (b) a 10% hematocrit (the ratio of the volume of RBCs to the total volume of blood) solution of a goat for testing (a goat blood sample was selected because of its similarity with human blood and then diluted with 0.9 wt% normal salines.), (c) an enlarged view of the network showing areas clogged by RBCs, and (d)–(f) the effects of enhanced pressure drop with an increase in flow rate to push clogged RBCs away. Reproduced from Chen *et al* (2010), with permission from Springer Nature.

arterioles and venules that deliver specific amounts of blood and its components throughout the human body. Chen *et al* (2010) designed a capillary network and employed μPIV to observe the deformability of red blood cells (RBCs) in capillaries and the effect of a higher pressure drop on pushing away some of the clogging RBCs through the blocked capillaries (figure 10). A cell-free layer (i.e. a thin layer adjacent to the wall without the presence of RBCs) within the capillaries was not detected because of the extremely small capillary sizes of 5 and 8 μm. This layer is of interest when the capillary size varies from 10 to 100 μm, and the physical forces push the RBCs to the center of the capillaries (e.g. Suggi *et al* 2005, Faivre *et al* 2006, Kim *et al* 2006a, Kim *et al* 2006b, 2009, Zhang *et al* 2009).

Micro-resolution PIV and PTV have become robust techniques for visualizing the flow dynamics of coughing and sneezing. These multicomponent human-generated exhalations include a wide range of droplet sizes, varying from 0.1 to 1 mm. Consequently, the social distance (i.e. the safe distance between a patient and a health care worker) can be determined by visualizing such flow and estimating the motion of pathogen-laden droplets. Table 6 presents the main findings of several recent μPIV measurements of sneezing, coughing, and speech. None of the studies mentioned in this table considered the presence of a medical/non-medical face mask which is a critical factor affecting airborne droplet spreading in terms of velocity and traveling distance (e.g. refer to Tang *et al* 2009, Dbouk and Drikakis 2020 for further information on droplet visualization in the presence of a face mask).

Micromixers have been designed to enhance the mixing rate in microfluidic devices through active and passive techniques. An active technique uses an external source of energy, e.g. electricity and magnetic fields, and a passive technique uses pressure or barriers (Santana *et al* 2015). μPIV can visualize and measure the velocity field in such pressure-driven flow through micromixers. Kim and Kihm (2004) introduced rectangular barriers embedded with a micromixer to produce a helical type of flow, and soon after, the idea was employed by Wang *et al* (2006), which resulted in a significant variation of velocity gradients and an improved mixing rate using μPIV. These advantages led to the miniaturization of the size of the microdevice, shortening the processing time, and minimizing the volume of fluids involved in the microchemistry processes.

Table 6. Summary of recent studies on the μPIV flow visualization of sneezing, coughing, and speaking.

References	Main findings regarding horizontal distance
Zhu *et al* (2006)	• The maximum horizontal traveling distance is more than 2 m for saliva droplets. • The highest velocity was 22 m s^{-1}. • The effects of inertia and gravity were insignificant for droplets smaller than 30 μm. • Gravity effects were more significant than inertia on droplets larger than 300 μm.
Chao *et al* (2009)	• Mean exhalation velocity was 11.7 m s^{-1} for coughing and 3.9 m s^{-1} for speaking. • Mean diameter of droplets were 13.5 μm and 16 μm for coughing and speaking, respectively. • A combined method of interferometric Mie imaging and PIV to measure droplet size and velocity, respectively.
Feng *et al* (2015)	• The use of a phase-averaged method due to the transient and periodic nature of breathing. • Bell-shaped and flat velocity distribution for exhalation and inhalation, respectively.
Wei and Li (2017)	• The use of two-stage cough flow called starting- and interrupted-jet stages instead of real human subject exhalations. • The maximum horizontal penetration distance is almost 50.6–85.5 times the diameter. • Maximum droplet velocity is around 10 m s^{-1}.
Bahl *et al* (2020)	• More than 99% of generated droplets move with a velocity of less than 10 m s^{-1}. • Near 20% of droplets travel at a velocity greater than 5 m s^{-1}. • Maximum droplet velocities vary from 12 to 15 m s^{-1}. • Probability distribution of droplets with a velocity of 2 m s^{-1} within 0–5 cm from the mouth is 70% and 36% greater than that for 10–15 cm and 20–25 cm, respectively.
Dudalski *et al* (2020)	• Cough averaged peak velocity magnitudes are 1.09, 1.01, and 1.22 m s^{-1} during sick, convalescent, and healthy stages of human subject. • Cough averaged velocity is 1.17 m s^{-1} at 1 m downstream. • The average spread angle is 24°. • Insignificant differences between coughs of sick and healthy participants in terms of the velocity and turbulence intensity.
Tan *et al* (2021)	• Plosive consonants with a stop, such as '*t*' and coughing, produce faster air jets compared to non-plosive consonants without a stop, such as '*s*' and '*m*'. • Horizontal traveling distance for plosive consonants are about 100 times the diameter of the mouth opening, which is significantly greater than that of 20 for non-plosive consonants. • A 2 m physical distancing (i.e. social distancing) can be destroyed under favorable conditions during speaking compared to coughing. • Droplet sizes vary from 0.1 to 1 μm and 10–100 μm for speech and cough, respectively.

4. Conclusions and outlooks

This study aimed to provide an in-depth understanding of the recent developments of PIVs and μPIVs and to highlight several novel measurement approaches to estimate the velocity vector field. The significant development of microscale flow visualization in terms of method, technology, and sustainability has made μPIV a precise and robust technique to quantify and describe flow structure. In this paper, two types of flow visualization methods: surface and off-the-surface were reviewed. Three off-the-surface techniques were then compared: shadowgraphy, schlieren, and interferometry. The recent PIV developments were studied in two well-known journals and then placed into three categories: theoretical (method), technological, and applicability, which were later used to show μPIV development. The CC method and its appreciable improvement using a regularization term were explained to consider the differences between several regularization terms found in the literature. Finally, the capability of μPIV measurements in bio-applications were discussed due to a tremendous interest in using this technology after the COVID-19 global pandemic.

The systematic overview of this study could be a reference to showcase how pre- and postprocessing techniques improve the velocity field reconstruction using ML techniques and as a resource for those who wish to inquire about advances happening to microscale flow visualization.

Data availability statement

The data that support the findings of this study are available upon reasonable request from the authors.

Acknowledgments

The authors acknowledge the financial support from the Natural Sciences and Engineering Research Council of Canada (NSERC) Grants 200439 and 209780 for funding this research.

Disclaimer

The equipment or commercial instruments identified here are only to ensure the integrity of the information. Such

identification does not imply recommendation or endorsement by the author, nor does it imply that the identified equipment is necessarily the best available for this purpose.

Conflict of interest

The authors declare no conflict of interest.

ORCID iD

Amin Etminan https://orcid.org/0000-0003-0173-7939

References

Adrian R J 1988 Double exposure, multiple-field particle image velocimetry for turbulent probability density *Opt. Lasers Eng.* **9** 211–28

Adrian R J and Westerweel J 2011 *Particle Image Velocimetry* (Cambridge: Cambridge University Press)

Akbari G and Montazerin N 2022 Reconstruction of particle image velocimetry data using flow-based features and validation index: a machine learning approach *Meas. Sci. Technol.* **33** 015203

Bahl P, de Silva C M, Chughtai A A, Maclntyre C R and Doolan C 2020 An experimental framework to capture the flow dynamics of droplets expelled by a sneeze *Exp. Fluids* **61** 176

Baker J L and Einav I 2021 Deep velocimetry: extracting full velocity distributions from projected images of flowing media *Exp. Fluids* **62** 102

Barzegar Gerdroodbary M 2020 Injection and mixing of single fuel jet *Scramjets, Fuel Mixing and Injection Systems* (Oxford: Butterworth-Heinemann) ch 3 pp 39–126

Beebe D J, Adrian R J, Olsen M G, Stremler M A, Aref H and Jo B H 2001 Passive mixing in microchannels: fabrication and flow experiments *Mec. Ind.* **2** 343–8

Blahout S, Reinecke S R, Kruggel-Emden H and Hussong J 2021 On the micro-PIV accuracy and reliability utilizing non-Gaussian particle images *Exp. Fluids* **62** 191

Brunton S L, Noack B R and Koumoutsakos P 2020 Machine learning for fluid mechanics *Annu. Rev. Fluid Mech.* **52** 477–508

Chao C Y H *et al* 2009 Characterization of expiration air jets and droplet size distributions immediately at the mouth opening *J. Aerosol. Sci.* **40** 122–33

Chen Y C, Chen G Y, Lin Y C and Wang G J 2010 A lab-on-a-chip capillary network for red blood cell hydrodynamics *Microfluid. Nanofluidics* **9** 585–91

Chun-Yu G, Yi-Wei F, Yang H, Peng X and Yun-Fei K 2021 Deep-learning-based liquid extraction algorithm for particle image velocimetry in two-phase flow experiments of an object entering water *Appl. Ocean Res.* **108** 102526

Cierpka C, Otto H, Poll C, Hüther J, Jeschke S and Mäder P 2021 SmartPIV: flow velocity estimates by smartphones for education and field studies *Exp. Fluids* **62** 172

Corpetti T, Heitz D, Arroyo G, Mémin E and Santa-Cruz A 2006 Fluid experimental flow estimation based on an optical-flow scheme *Exp. Fluids* **40** 80–97

Corpetti T, Mémin E and Pérez P 2002 Dense estimation of fluid flows *IEEE Trans. Pattern Anal. Mach. Intell.* **24** 365–80

Dbouk T and Drikakis D 2020 On respiratory droplets and face masks *Phys. Fluids* **32** 063303

de Silva C M, Bahl P, Doolan C and Maclntyre C R 2021 Bespoke flow experiments to capture the dynamics of coughs and sneezes *Meas. Sci. Technol.* **32** 125302

Dudalski N, Mohamed A, Mubareka S, Bi R, Zhang C and Savory E 2020 Experimental investigation of far-field human cough airflows from healthy and influenza-infected subjects *Indoor Air* **30** 966–77

Duffy D C, Gillis H L, Lin J, Sheppard N F and Kellogg G J 1999 Microfabricated centrifugal microfluidic systems: characterization and multiple enzymatic assays *Anal. Chem.* **71** 4669–78

Eck M, Rückert R and Peitsch D 2019 Advanced application of a sublayer fence probe in highly instationary turbomachinery flows: observations on prestall instabilities *Exp. Fluids* **60** 47

Elsinga G E, Scarano F, Wieneke B and van Oudheusden B W 2006 Tomographic particle image velocimetry *Exp. Fluids* **41** 933–47

Fahringer T W, Lynch K P and Thurow B S 2015 Volumetric particle image velocimetry with a single plenoptic camera *Meas. Sci. Technol.* **26** 115201

Faivre M, Abkarian M, Bickraj K and Stone H A 2006 Geometrical focusing of cells in a microfluidic device: an approach to separate blood plasma *Biorheology* **43** 147–59

Feng L, Yao S, Sun H, Jiang N and Liu J 2015 TR-PIV measurement of exhaled flow using a breathing thermal manikin *Build. Environ.* **94** 683–93

George W K and Stanislas M 2021 On the noise in statistics of PIV measurements *Exp. Fluids* **62** 188

Ghouila-Houri C, Gallas Q, Garnier E, Merlen A, Viard R, Talbi A and Pernod P 2017 High temperature gradient calorimetric wall shear stress micro-sensor for flow separation detection *Sens. Actuators* A **266** 232–41

Ghouila-Houri C, Talbi A, Viard R, Gallas Q, Garnier E, Merlen A and Pernod P 2019a High temperature gradient micro-sensors array for flow separation detection and control *Smart Mater. Struct.* **28** 125003

Ghouila-Houri C, Talbi A, Viard R, Gallas Q, Garnier E, Merlen A and Pernod P 2019b Unsteady flows measurements using a calorimetric wall shear stress micro-sensor *Exp. Fluids* **60** 67

Ghouila-Houri C, Talbi A, Viard R, Gallas Q, Garnier E, Molton P, Delva J, Merlen A and Pernod P 2021 MEMS high temperature gradient sensor for skin-friction measurements in highly turbulent flows *IEEE Sens. J.* **21** 9749–55

Gu P H, Chen J and Wang D Z C 2021 Reconstructing unsteady flow data from representative streamlines via diffusion and deep learning based denoising *IEEE Comput. Graph. Appl.* **41** 111–21

Haffner E A, Bagheri M, Higham J E, Cooper L, Rowan S, Stanford C, Mashayek F and Mirbod P 2021 An experimental approach to analyze aerosol and splatter formations due to a dental procedure *Exp. Fluids* **62** 202

Higham J, Brevis W and Keylock C J 2016 A rapid non-iterative proper orthogonal decomposition based outlier detection and correction for PIV data *Meas. Sci. Technol.* **27** 125303

Horn B K P and Schunck B G 1981 Determining optical flow *Artif. Intell.* **17** 185–203

Kadri-Harouna S, Dérian P, Héas P and Mémin E 2013 Divergence-free wavelets and high order regularization *Int. J. Comput. Vis.* **103** 80–99

Keane R D and Adrian R J 1992 Theory of cross-correlation analysis of PIV images *Appl. Sci. Res.* **49** 191–215

Kim K C 2012 Advances and applications on micro-defocusing digital particle image velocimetry (μ-DDPIV) techniques for microfluidics *J. Mechan. Sci. Technol.* **26** 3769–84

Kim M J and Kihm K D 2004 Microscopic PIV measurements for electro-osmotic flows in PDMS microchannels *J. Vis.* **7** 111–8

Kim S, Kong R L, Popel A S, Intaglietta M and Johnson P C 2006a A computer-based method for determination of the cell-free layer width in microcirculation *Microcirculation* **13** 199–207

Kim S, Kong R L, Popel A S, Intaglietta M and Johnson P C 2006b Temporal and spatial variations of cell-free layer width in arterioles *Am. J. Physiol. Heart Circ. Physiol.* **293** H1526–35

Kim S, Ong P K, Yalcin O, Intaglietta M and Johnson P C 2009 The cell-free layer in microvascular blood flow *Biorheology* **46** 181–9

Kirby B J 2010 *Micro- and Nanoscale Fluid Mechanics: Transport in Microfluidic Devices* (Cambridge: Cambridge University Press)

Kislaya A, Deka A, Veenstra P, Tam D S W and Westerweel J 2020 Psi-PIV: a novel framework to study unsteady microfluidic flow *Exp. Fluids* **61** 20

Kreizer M, Ratner D and Liberzon A 2010 Real-time image processing for particle tracking velocimetry *Exp. Fluids* **48** 105–10

Krizhevsky A, Sutskever I and Hinton G E 2012 ImageNet classification with deep convolutional neural networks *Adv. Neural Inf. Process. Syst.* **25** 1097–105

Lagemann C, Lagemann K, Mukherjee S and Schröder W 2021 Deep recurrent optical flow learning for particle image velocimetry data *Nat. Mach. Intell.* **3** 641–51

Lee Y, Yang H and Yin Z 2017 PIV-DCNN: cascaded deep convolutional neural networks for particle image velocimetry *Exp. Fluid* **58** 171

Liu T, Merat A, Makhmalbaf M H M, Fajardo C and Merati P 2015 Comparison between optical flow and cross-correlation methods for extraction of velocity fields from particle images *Exp. Fluids* **56** 166

Løken T K, Ellevold T J, de la Torre R G R, Rabault J and Jensen A 2021 Bringing optical fluid motion analysis to the field: a methodology using an open source ROV as a camera system and rising bubbles as tracers *Meas. Sci. Technol.* **32** 095302

Lu J, Yang H, Zhang Q and Yin Z 2021 An accurate optical flow estimation of PIV using fluid velocity decomposition *Exp. Fluids* **62** 78

Lumley J L 1981 Coherent structures in turbulence *Transition and Turbulence* pp 215–42

Meinhart C D, Wereley S T and Santiago J G 1999 PIV measurements of a micro-channel flow *Exp. Fluids* **27** 414–9

Meinhart C D, Wereley S T and Santiago J G 2000 A PIV algorithm for estimating time-averaged velocity fields *ASME, J. Fluids Eng.* **122** 285–9

Merzkirch W 1987 *Flow Visualization* 2nd edn (New York: Academic)

Merzkirch W and Ramesh N 2000 The role of color in the optical visualization of flows with variable fluid density *Science and Art Symposium* ed A Gyr, P D Koumoutsakos and U Burr (Dordrecht: Springer)

Nagel H-H and Enkelmann W 1986 An investigation of smoothness constraints for the estimation of displacement vector fields from image sequences *IEEE Trans. Pattern Anal. Mach. Intell.* **8** 565–93

Noto D and Tasaka Y 2021 Dual-plane ensemble correlation for pixelwise 2D-3C velocity field measurements using a single camera *Exp. Fluids* **62** 111

Olsen M G and Adrian R J 2000 Brownian motion and correlation in particle image velocimetry *Opt. Laser Technol.* **32** 621–7

Olsen M G and Adrian R J 2001 Out-of-focus effects on particle image visibility and correlation in microscopic particle image velocimetry *Exp. Fluids* **29** S166–74

Paris S, Hasinoff S W and Kautz J 2011 Local Laplacian filters: edge-aware image processing with a Laplacian pyramid *ACM Trans. Graph.* **30** 68

Patel V C 1965 Calibration of the Preston tube and limitations on its use in pressure gradients *J. Fluid Mech.* **23** 185–208

Pereira F and Gharib M 2002 Defocusing digital particle image velocimetry and the three-dimensional characterization of two-phase flows *Meas. Sci. Technol.* **13** 683–94

Pereira F, Lu J, Castaño-Graff E and Gharib M 2007 Microscale 3D flow mapping with μDDPIV *Exp. Fluids* **40** 589–99

Quénot G, Pakleza J and Kowalewski T A 1998 Particle image velocimetry with optical flow *Exp. Fluid* **25** 177–89

Rabault J, Kolaas J and Jensen A 2017 Performing particle image velocimetry using artificial neural networks: a proof-of-concept *Meas. Sci. Technol.* **28** 125301

Raffel M, Willert C E, Scarano F, Kähler C J, Wereley S T and Kompenhans J 2018 *Particle Image Velocimetry a Practical Guide* 3rd edn (Switzerland: Springer)

Rezende D J and Mohamed S 2015 Variational inference with normalizing flows *Proc. 32nd Int. Conf. on Machine Learning* (*Lille, France*)

Rice B E, McKenzie J A, Peltier S J, Combs C S, Thurow B S, Clifford C J and Johnson K 2018 Comparison of 4-camera tomographic PIV and single-camera plenoptic PIV *Proc. 56th AIAA Aerospace Sciences Meeting* (*Kissimmee, FL*)

Ristić S 2007 Flow visualization techniques in wind tunnels, part I-non optical method *Sci. Tech. Rev.* **57** 39–50

Ruhnau P, Kohlberger T, Schnörr C and Nobach H 2005 Variational optical flow estimation for particle image velocimetry *Exp. Fluid* **38** 21–32

Saad M R 2013 Experimental studies on shock boundary layer interactions using micro-ramps at Mach 5 *PhD Thesis* The University of Manchester, United Kingdom

Saini P, Arndt C M and Steinberg A M 2016 Development and evaluation of gappy-POD as a data reconstruction technique for noisy PIV measurements in gas turbine combustors *Exp. Fluids* **57** 122

Santana H S, Silva J L Jr and Taranto O P 2015 Numerical simulation of mixing and reaction of *Jatropha curcas* oil and ethanol for synthesis of biodiesel in micromixers *Chem. Eng. Sci.* **132** 159–68

Santiago J G, Wereley S T, Meinhart C D, Beebe D J and Adrian R J 1998 A particle image velocimetry system for microfluidics *Exp. Fluids* **25** 316–9

Scarano F 2002 Iterative image deformation methods in PIV *Meas. Sci. Technol.* **13** R1–19

Scarano F 2012 Tomographic PIV: principles and practice *Meas. Sci. Technol.* **24** 012001

Schmidt B E and Sutton J A 2020 Improvements in the accuracy of wavelet-based optical flow velocimetry (wOFV) using an efficient and physically based implementation of velocity regularization *Exp. Fluids* **61** 32

Schmidt B E and Sutton J A 2021 A physical interpretation of regularization for optical flow methods in fluids *Exp. Fluids* **62** 34

Schober M, Obermaier E, Pirskawetz S and Fernholz H H 2004 A MEMS skin-friction sensor for time resolved measurements in separated flows *Exp. Fluids* **36** 593–9

Schroeder A and Willert C E 2008 *Particle Image Velocimetry New Developments and Recent Applications* (Berlin: Springer-Verlag)

Seong J H, Song M S, Nunez D, Manera A and Kim E S 2019 Velocity refinement of PIV using global optical flow *Exp. Fluids* **60** 174

Settles G S 2001 *Schlieren and Shadowgraph Techniques: Visualizing Phenomena in Transparent Media* (Berlin: Springer)

Shi S, Ding J, Atkinson C, Soria J and New T H 2018 A detailed comparison of single-camera light-field PIV and tomographic PIV *Exp. Fluids* **59** 46

Shi S, Wang J, Ding J, Zhao Z and New T H 2016 Parametric study on light field volumetric particle image velocimetry *Flow Meas. Instrum.* **49** 70–88

Simonini A, Theunissen R, Masullo A and Vetrano M R 2019 PIV adaptive interrogation and sampling with image projection applied to water sloshing *Exp. Therm. Fluid Sci.* **102** 559–74

Smits A J and Lim T T 2012 *Flow Visualization: Techniques and Examples* (London: Imperial College Press)

Stevens P R R J and Sciacchitano A 2021 Application of clustering and the Hungarian algorithm to the problem of consistent vortex tracking in incompressible flowfields *Exp. Fluids* **62** 173

Sugii Y, Okuda R, Okamoto K and Madarame H 2005 Velocity measurement of both red blood cells and plasma of *in vitro* blood flow using high-speed micro PIV technique *Meas. Sci. Technol.* **16** 1126–30

Tan Z P, Silwal L, Bhatt S P and Raghav V 2021 Experimental characterization of speech aerosol dispersion dynamics *Sci. Rep.* **11** 3953

Tang J W, Liebner T J, Craven B A and Settles G S 2009 A schlieren optical study of the human cough with and without wearing masks for aerosol infection control *J. R. Soc. Interface* **6** S727

von Papen T, Steffes H, Ngo H D and Obermeier E 2002 A micro surface fence probe for the application in flow reversal areas *Sens. Actuators* A **97–98** 264–70

Wang R J, Lin J Z and Xie H B 2006 Velocity measurement of flow in the microchannel with barriers using micro-PIV *J. Vis.* **9** 209–17

Wei J and Li Y 2017 Human cough as a two-stage jet and its role in particle transport *PLoS One* **12** e0169235

Wen X, Li Z, Peng D, Zhou W and Liu Y 2019 Missing data recovery using data fusion of incomplete complementary data sets: a particle image velocimetry application *Phys. Fluids* **31** 025105

Westerweel J 1997 Fundamentals of digital particle image velocimetry *Meas. Sci. Technol.* **8** 1379–92

Westerweel J and Scarano F 2005 Universal outlier detection for PIV data *Exp. Fluids* **39** 1096–100

Whitesides G M, Ostuni E, Takayama S, Jiang X and Ingber D E 2001 Soft lithography in biology and biochemistry *Annu. Rev. Biomed. Eng.* **3** 335–73

Willert C E and Gharib M 1991 Digital particle image velocimetry *Exp. Fluids* **10** 181–93

Willert C E and Gharib M 1992 Three-dimensional particle imaging with a single camera *Exp. Fluids* **12** 353–8

Xiong J, Aguirre-Pablo A A, Idoughi R, Thoroddsen S T and Heidrich W 2021 RainbowPIV with improved depth resolution—design and comparative study with TomoPIV *Meas. Sci. Technol.* **32** 025401

Xiong J, Idoughi R, Aguirre-Pablo A A, Aljedaani A B, Dun X, Fu Q, Thoroddsen S T and Heidrich W 2017 Rainbow particle imaging velocimetry for dense 3D fluid velocity imaging *ACM Trans. Graph.* **36** 1–14

Yang X and Zhang M 2021 Review of flexible microelectromechanical system sensors and devices *Nanotechnol. Precis. Eng.* **4** 025001

Yoon S Y and Kim K C 2006 3D particle position and 3D velocity field measurement in a microvolume via the defocusing concept *Meas. Sci. Technol.* **17** 2897–905

Yu C D, Fan Y W, Bi X J, Han Y and Kuai Y F 2021 Deep particle image velocimetry supervised learning under light conditions *Flow Meas. Instrum.* **80** 102000

Yuan J, Schnörr C and Mémin E 2007 Discrete orthogonal decomposition and variational fluid flow estimation *J. Math Imaging Vis.* **28** 67–80

Zhang J, Johnson P C and Popel A S 2009 Effects of erythrocyte deformability and aggregation on the cell free layer and apparent viscosity of microscopic blood flows *Microvasc. Res.* **77** 265–72

Zhu S, Kato S and Yang J H 2006 Study on transport characteristics of saliva droplets produced by coughing in a calm indoor environment *Build. Environ.* **41** 1691–702

Zitová B and Flusser J 2003 Image registration methods: a survey *Image Vis. Comput.* **21** 977–1000